Ground motion modelling updates applicable to seismic hazard assessments for dams in Australia

Jeff Bayless, Paul Somerville, and Hong Kie Thio
AECOM, 300 South Grand Ave, Los Angeles, CA 90071, United States of America

For all categories of dams, the ANCOLD (2019) guidelines specify how a seismic hazard assessment (SHA) should be performed. One critical component of a SHA is the selection of ground motions models (GMMs), as described in Section 2.5 of ANCOLD (2019), because the SHA results are highly dependent on these models. The Somerville et al. (2009; Sea09) GMMs for Australia are due to be improved by taking advantage of ground motions recorded in the past decade-plus. Changes to seismic hazard models with time reflect our increasing knowledge of earthquake source and ground motion characteristics in Australia. This paper describes how the Sea09 ground motion model has changed, and as a result how SHA results for dam projects may be impacted. Comparisons with recently recorded ground motions in Australia have revealed that refinements to the distance and depth scaling components of the model provide a better fit to those data. This update also involves ongoing earthquake ground motion simulations; these are validated using the recorded ground motion data and are used to extrapolate the model to larger earthquake magnitudes that typically control design ground motions but for which no Australian data are available.

Keywords: seismic hazard assessments, ground motion modelling

Introduction

For all categories of dams, the ANCOLD (2019) guidelines specify how a seismic hazard assessment (SHA) should be performed. One critical component of a SHA is the selection of ground motions models (GMMs), as described in Section 2.5 of ANCOLD (2019), because the SHA results are highly dependent on these models.

The Somerville et al. (2009; Sea09) GMMs for Australia were based on ground motion simulations, and then checked for consistency with the recorded ground motions of the moment magnitude (**M**) 4.47 Thompson Reservoir earthquake of 1996. In the course of the National Seismic Hazard Assessment (NSHA18; Allen et al., 2018), Geoscience Australia assessed the performance of existing ground motion models in predicting recorded ground motions in Australia (Ghasemi and Allen, 2018). They demonstrated that Sea09 could be improved by taking advantage of ground motions recorded in the past decade-plus. The expectation of change in ground motion models is embodied in ANCOLD Section 2.5, which states that it is unlikely that a SHA more than about 10 years old is reliable. Changes to seismic hazard models with time reflect our increasing knowledge of earthquake source and ground motion characteristics in Australia.

This paper describes how the Sea09 ground motion model has changed, and as a result how SHA results for dam projects may be impacted. Comparisons with recently recorded ground motions in Australia have revealed that refinements to the distance and depth scaling components of the model provide a better fit to those data. This update also involves ongoing earthquake ground motion simulations; these are validated using the recorded ground motion data and are used to extrapolate the model to larger earthquake magnitudes that typically control design ground motions but for which no Australian data are available.

Earthquake Data

Cratonic Earthquake Ground Motions

We compiled a Cratonic earthquake ground motion database including waveform data from Geoscience Australia (Allen and Ghasemi, 2020), who provided instrument corrected recordings for events occurring within Cratonic regions, and from IRIS (https://ds.iris.edu/wilber3/). We removed events with **M** less than 3.0, recordings with distance greater than 600 km, and those identified as clipped, with poor signal to noise ratio, or other artifacts. Recordings without both orthogonal horizontal components were also removed. The resulting database contains 536, homogeneously processed, ground motion records from 83 events recorded by 143 unique stations.

The Cratonic ground motion database includes three earthquakes with more than 80 recorded ground motions, these are the **M**3.91 event on 2019 May 30, the **M**4.71 event on 2019 May 5, and the **M**4.96 event on 2019 August 1. These three earthquakes were located within the Northern Australian Craton and were recorded by the temporary AusARRAY deployment (Gorbatov et al., 2020). The remaining 80 earthquakes in the database have fewer than 10 recordings. There are 34 total events with $\mathbf{M} \geq 4.0$ and 33 events with $3.5 \leq \mathbf{M} < 4.0$. The 5% damped, horizontal component pseudo-spectral accelerations (RotD50) are calculated from two-component band-passed acceleration time histories using the pyRotd python library (Kottke, 2018).

Source Inversions

The cut-and-paste (CAP) method for retrieving earthquake source parameters (Zhao and Helmberger, 1994; Tan et al., 2010) breaks three-component data into *Pnl* and surface wave segments and models them separately, so imperfect 1-dimensional Green's functions can be effectively used to determine source parameters. We utilize this method on the events listed in Table 1 to improve our estimates of **M**, focal depth, focal mechanism, and location. Figure 1 shows the results of this method, using a six-station inversion, for the August 1, 2019 Northern Territory event. This inversion has a minimum waveform misfit error at 2 km depth (centre left panel), and a northeast p-axis orientation consistent with Hillis & Reynolds (2000) (top left). The event and recording station locations are shown in the bottom left panel, and the fits between the recorded (red) and synthetic (blue) waveforms are shown on the right.

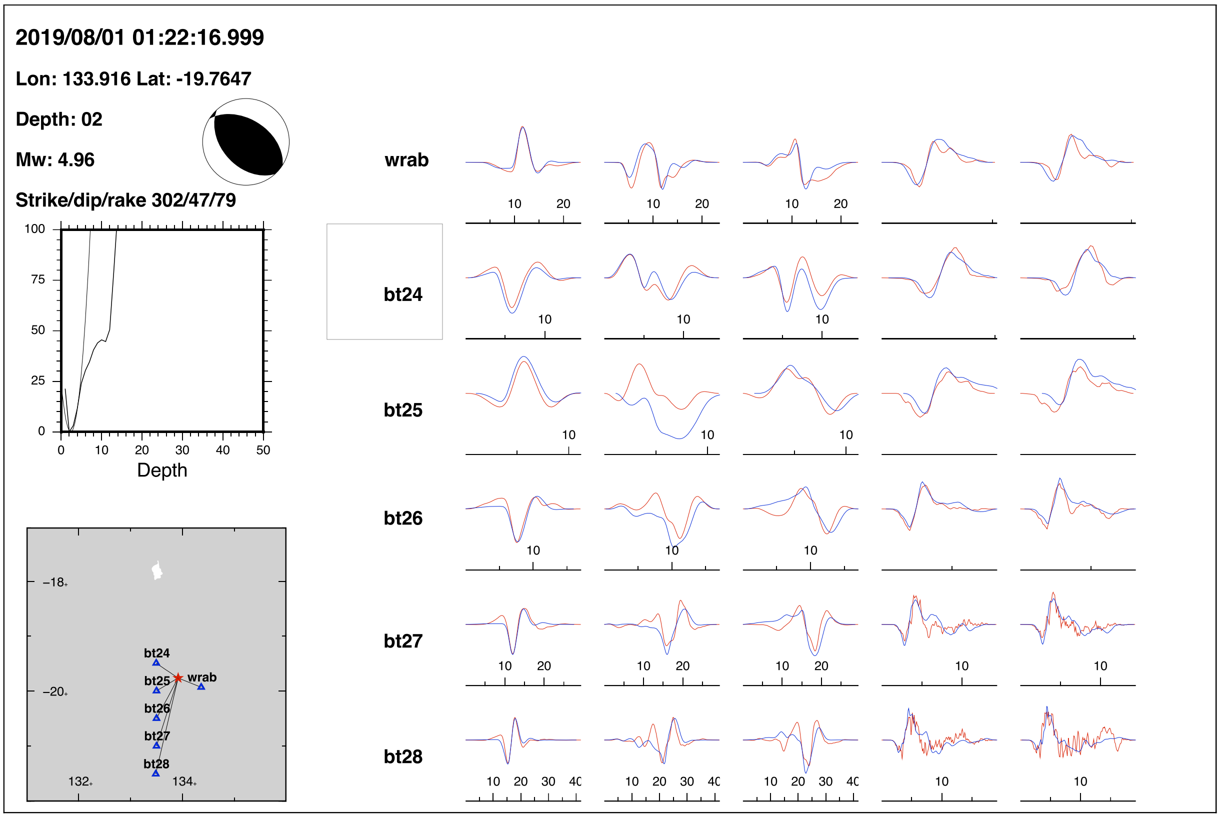

Figure 1. CAP method results for the 2019/08/01 earthquake in the NT.

Table 1. Cratonic region earthquakes. Values for EQIDs 13, 49, and 55 (italicized) are from Geoscience Australia.

EQID	M	Date	Epicenter Longitude (deg)	Epicenter Latitude (deg)	Hypocenter Depth (km)	Strike, Rake, Dip (deg)	Region	No. of Usable 2-component Recordings
61	4.96	2019-08-01	133.916	-19.7647	2	302, 47, 79	Northern Aus Craton	98
59	4.71	2019-05-30	131.85876	-21.28147	5	103, 59, 14	Northern Aus Craton	83
60	3.91	2019-05-30	131.92337	-21.32752	4	101, 64, 3	Northern Aus Craton	85
58	5.34	2018-11-08	116.78733	-34.42316	9	151, 90, 52	Yilgarn Craton	5
53	4.90	2018-09-16	116.78	-34.43	7	347, 53, 44	Yilgarn Craton	6
44	4.91	2016-07-08	122.511	-32.458	5	331, 37, 59	Yilgarn Craton	6
13	*4.6*	*2020-03-30*	*117.049*	*-30.519*	*0.8*	-,-,-	*Yilgarn Craton*	*8*
55	*4.54*	*2018-10-12*	*116.79882*	*-34.39522*	*5.8*	-,-,-	*Yilgarn Craton*	*8*
49	*4.13*	*2017-01-03*	*118.455*	*-30.609*	*10*	-,-,-	*Yilgarn Craton*	*9*
72	4.39	2010-06-05	136.796	-33.5949	23	0, 62, 51	Gawler Craton	5
82	3.53	2018-07-01	136.7729	-33.618	23	209, 38, 51	Gawler Craton	5
83	4.41	2018-11-21	136.923	-33.2585	33	319, 32, -83	Gawler Craton	5

Empirical Calibration

The need to adjust Sea09 is based on evaluations of the performance of the model compared with the earthquake ground motion data. Figure 2 shows an example of this observation for the **M**4.71 earthquake on May 30, 2019. In the top panel, the peak ground acceleration (PGA) versus distance predicted by the Sea09 Cratonic earthquake model is compared with the recordings, where the data are adjusted to the Vs30=865 m/s condition for consistency with Sea09. Figure 2 shows that the Sea09 model overpredicts at close distances and underpredicts at large distances. The bottom panel of Figure 2 shows ground motion residuals calculated from the Sea09 model, and the linear trend in these residuals also illustrates the difference in PGA attenuation for this event with that assumed in Sea09. Figure 3 shows a map of the earthquake location and recording sites, along with the boundary between the Northern Australian Craton to the north, and the reactivated Proterozoic crust to the south. Sites within the Cratonic region boundary are filled circles in Figure 1, and sites outside the boundary are white squares. Similar behaviour is observed for the other Cratonic region events for which we have recorded data. Additionally, the fact that the Sea09 Cratonic ground motion model has a more rapid decay with distance than the non-Cratonic model (not shown), which is the opposite of what we would expect, is an indication that the Cratonic model needs adjustment.

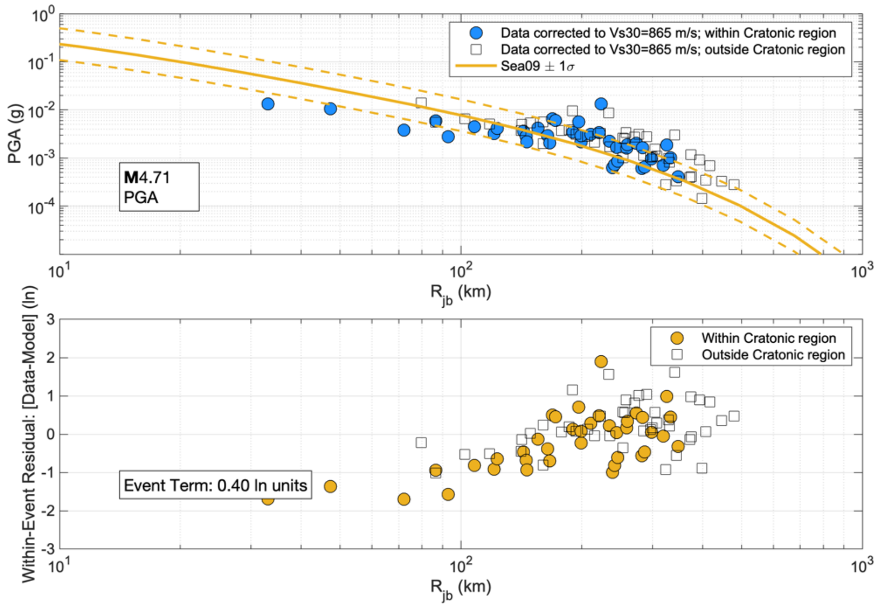

Figure 2. Evaluation of the Sea09 model with ground motion recordings of the May 30, 2019 M4.71 earthquake. Top: PGA versus distance. Bottom: Within-event residuals versus distance.

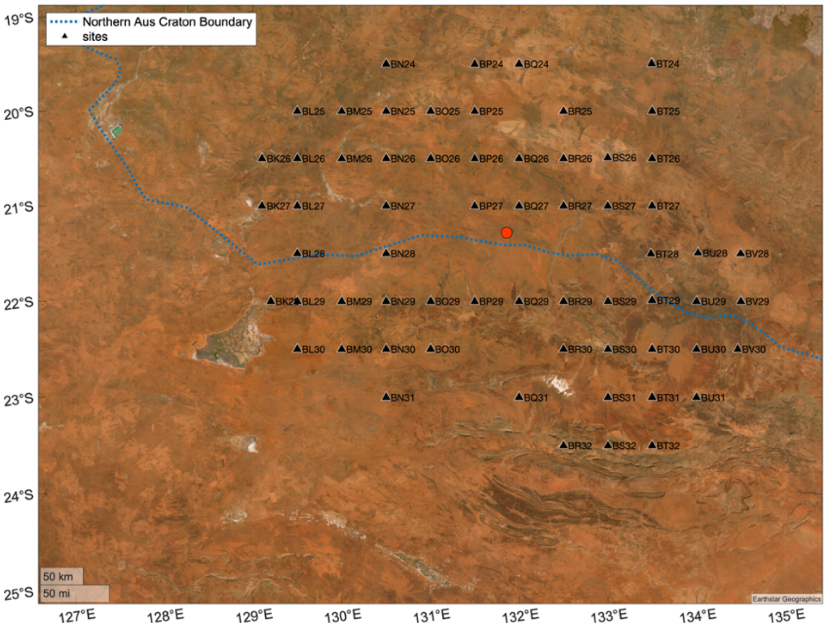

Figure 3. A satellite image map of the May 30, 2019 M4.71 earthquake epicentre (red circle) and recording stations (triangles). The blue dashed line represents the boundary between the Northern Australian Craton to the north, and the reactivated Proterozoic crust to the south.

The basic form of Sea09 follows Eq. 1:

$$\ln Sa = c_1 + c_2(\mathbf{M} - m_1) + c_3\ln R + c_4(\mathbf{M} - m_1)\ln R + c_5 r + c_8(8.5 - \mathbf{M})^2 \quad (1)$$

Where $c_3\ln R$ and $c_4(\mathbf{M} - m_1)\ln R$ represent the magnitude-independent and magnitude-dependent geometric spreading terms, respectively, and $c_5 r$ represents the anelastic attenuation (Q) term. In the terms that use the logarithm of distance (lnR), Sea09 uses $R = \sqrt{(R_{jb}^2 + h^2)}$ where R_{jb} is the Joyner-Boore distance in km and the constant h can be interpreted as a fictitious distance, which causes a flattening of the attenuation curve at very short distances due to the finite rupture dimensions. Sea09 found that a value of 6 km for h provided the best fit both for the Cratonic and Non-Cratonic models.

We update the Sea09 Cratonic model coefficients which control the decay with distance; the geometric spreading and anelastic attenuation model terms. The coefficient c_5 is revised by adding a period-dependent constant δc_5. The value of δc_5 ranges from $\delta c_5 = 0.0015$ at zero period (PGA) to $\delta c_5 = 0.0$ at 10 sec. Increasing c_5 results in more gradual attenuation of the ground motions at distances greater than approximately 80 km (reduced anelastic attenuation). The magnitude-independent geometric spreading coefficient, c_3, is adjusted by adding a period-dependent constant δc_3. The value of δc_3 ranges from $\delta c_3 = 0.2$ at zero seconds period (PGA) and reduces to $\delta c_3 = 0.0$ at ten seconds period, with linear slope in log-period space. Increasing c_3 has the effect of decreasing the attenuation (slope) of the ground motions with distance for distances less than about 80 km. The magnitude-dependent geometric spreading coefficient, c_4, is not modified at this stage because there are not enough large magnitude data to constrain it; the largest Cratonic earthquake with data is about **M**5.2. Finally, the constant c_1 is adjusted by adding $\delta c_1 = -(\delta c_3 + \delta c_5)\ln 100$. The constant adjustment is required because the other two adjustments (δc_3 and δc_5) each increase the predicted ground motion levels for all magnitudes and distances. To balance these, δc_1 hinges the revised model to the Sea09 model values at approximately 100 km distance based on the observation that the model generally does well in this distance range (e.g., Hoult et al., 2021; Bayless et al., 2022). The value of h is unchanged in the adjusted model.

The adjustments described above were set by observation of the attenuation and spectral shapes of the recordings of the earthquakes listed in Table 1. The period-dependence of δc_3 and δc_5 modifies the predicted spectral shape. The change in spectral shape is most pronounced at short distances, where the geometric spreading term dominates the attenuation, and at short periods, where the coefficient modifications are largest. The change in spectral shape is expressed as a reduction of the short period ground motions with minimal change in the long period ground motions.

Ground Motion Simulations

Ground motion simulations are used to extrapolate the model to larger earthquake magnitudes that typically control design ground motions but for which no Australian data are available. The earthquake ground motion simulations are validated using the recorded ground motion data. This portion of the Sea09 update is ongoing.

We use the hybrid broadband ground motion simulation methodology of Graves and Pitarka (2015; 2014; 2010; 2004; GP15) as implemented on the Southern California Earthquake Center Broadband Platform, version 19.8 (SCEC BBP; Maechling et al., 2015). The GP15 method combines a deterministic approach at low frequencies (f<1 Hz) with a semistochastic approach at high frequencies (f>1 Hz), where the broadband (0-10 Hz) response is obtained by summing the separate responses in the time domain using matched filters centred at 1 Hz. In GP15 the fault rupture is represented kinematically and incorporates spatial heterogeneity in slip, rupture speed, and rise time by discretising an extended finite-fault into a number of smaller subfaults. The GP15 prescribed slip distribution is constrained to follow an inverse wavenumber-squared fall-off and the average rupture speed is set at a fraction of the local shear-wave velocity, which is then adjusted such that the rupture propagates faster in regions of high slip and slower in regions of low slip. At low frequencies (f<1 Hz), the GP15 methodology contains a theoretically rigorous representation of fault rupture and wave propagation effects, and attempts to reproduce recorded ground motion waveforms and amplitudes by summing the response for many point sources distributed across each subfault. At high frequencies (f>1 Hz), GP15 uses a stochastic representation of source radiation, which is combined with a simplified theoretical representation of wave propagation and scattering effects for each subfault.

Graves and Pitarka (2015) extended their broadband simulation method from active region crustal earthquakes to earthquakes in stable continental regions based on findings from Somerville et al. (2009), Leonard (2010), Beresnev and Atkinson (2002), and with calibration using three eastern North America earthquakes. The modifications included: increasing the average rise time, reducing the average corner frequency, increasing the high frequency stress parameter, using the Leonard (2010) magnitude-area scaling relations, changing the high frequency attenuation (through kappa and Q models), changing the background rupture speed, and removing the shallow and deep weak zones from the rupture characterization (Graves and Pitarka, 2015). We use these parameter recommendations from Graves and Pitarka (2015) as a starting point and take a trial-and-error approach to refine the parameters based on the simulation and validation of earthquakes in Table 1. A summary of the final parameters and values required by the BBP v19.8 implementation of GP15 will be provided upon completion of the Sea09 update.

The simulations are performed for the events and recording stations listed in Table 1, using the GP method and with the Green's functions described in Bayless et al. (2022). The simulation results for the first event in Table 1 (EQID 61) are presented in this paper. The AusARRAY sites which recorded the EQID 61 earthquake, shown in Figure 4, are located near or within the Northern Australian Craton NSHA18 region, and their site conditions are poorly known. The uncertainties in Vs30 values and in the site response adjustments are significant and could be reduced in the future with additional data collection or improved models; these sources of uncertainty were similarly identified and accepted in NGA-East (Goulet et al., 2021).

For a given spectral period and recording station, the residual is defined as the difference between the natural logarithm of the recorded spectral acceleration (data) and the simulated spectral acceleration, after correcting for site conditions. Figure 4a shows a map of the within-event PGA residuals for this simulation, where negative residuals (cool colours) correspond to simulation over-prediction. Figure 4b shows the mean of spectral acceleration over all sites at each period; this compares the mean spectral shape of the simulations with the data. The dashed blue line in Figure 4b is the mean spectral shape after adjusting each site's recorded response spectrum to the Vs30=760 m/s condition using the Stewart et al (2021) site amplification model for stable continental regions. The small bump at about 1.5-2 seconds in the response spectra of both the simulations and the recordings is due to the R_g wave, which is caused by a shallow low velocity layer in the crust and which produces large peak ground velocities. Sea09 observed and modelled this ground motion feature.

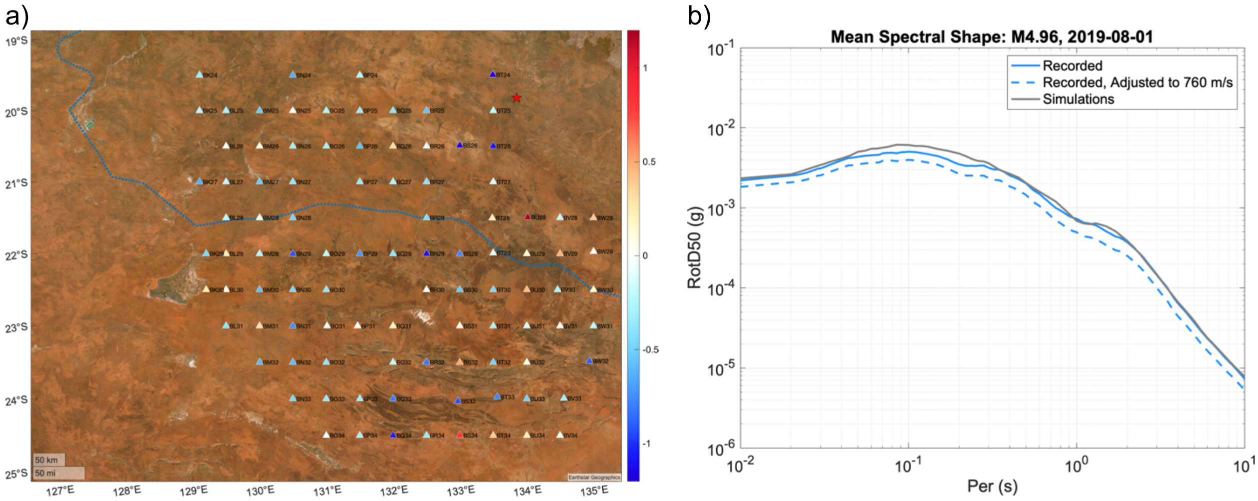

Figure 4. (a) A satellite image map showing color-coded within-event residuals at the recording sites with less than 600 km hypocentral distance. (b) Mean spectral shapes of all sites within 300 km, showing simulated, recorded, and recorded with adjustment to the Vs30=760 m/s site condition.

Figure 5 shows the distance attenuation of RotD50 spectral acceleration at all sites with less than 300 km rupture distance, for four periods: 0.01 sec (PGA), 0.2 sec, 1 sec, and 4 sec. The Sea09 median plus and minus one standard deviation model predictions are shown, and the circles represent stations inside the Cratonic region boundary, while squares represent stations outside of this boundary. Figure 5 illustrates good agreement in the distance scaling of the simulations with the data from this event.

Figure 6a shows the goodness-of-fit (GOF) summary for this earthquake simulation. The GOF is computed for each spectral period. The mean bias (black line) is the mean residual calculated from all recording stations, using the same definition of residual as defined previously. The red shaded area represents the 90% confidence interval in the mean bias and the green shaded area represents +/- 1 standard deviation among the residuals. The simulation of this event is over-predicted slightly across all periods without strong period dependence in the mean GOF; no period dependence is encouraging, and a mean bias is generally acceptable if some other events are systematically low, because each event is expected to have an event term. In the final stages of the simulations, the GOF of each event in Table 1 will be compared to determine if the simulations are acceptably calibrated to the recorded data.

Figure 6b shows displacement time series with rupture distance (vertical axis) for the simulations (left) and recordings (right) with less than 300 km rupture distance. Overall, there are strong similarities in the amplitudes, phasing, and durations of the waveforms between the simulations and the recordings.

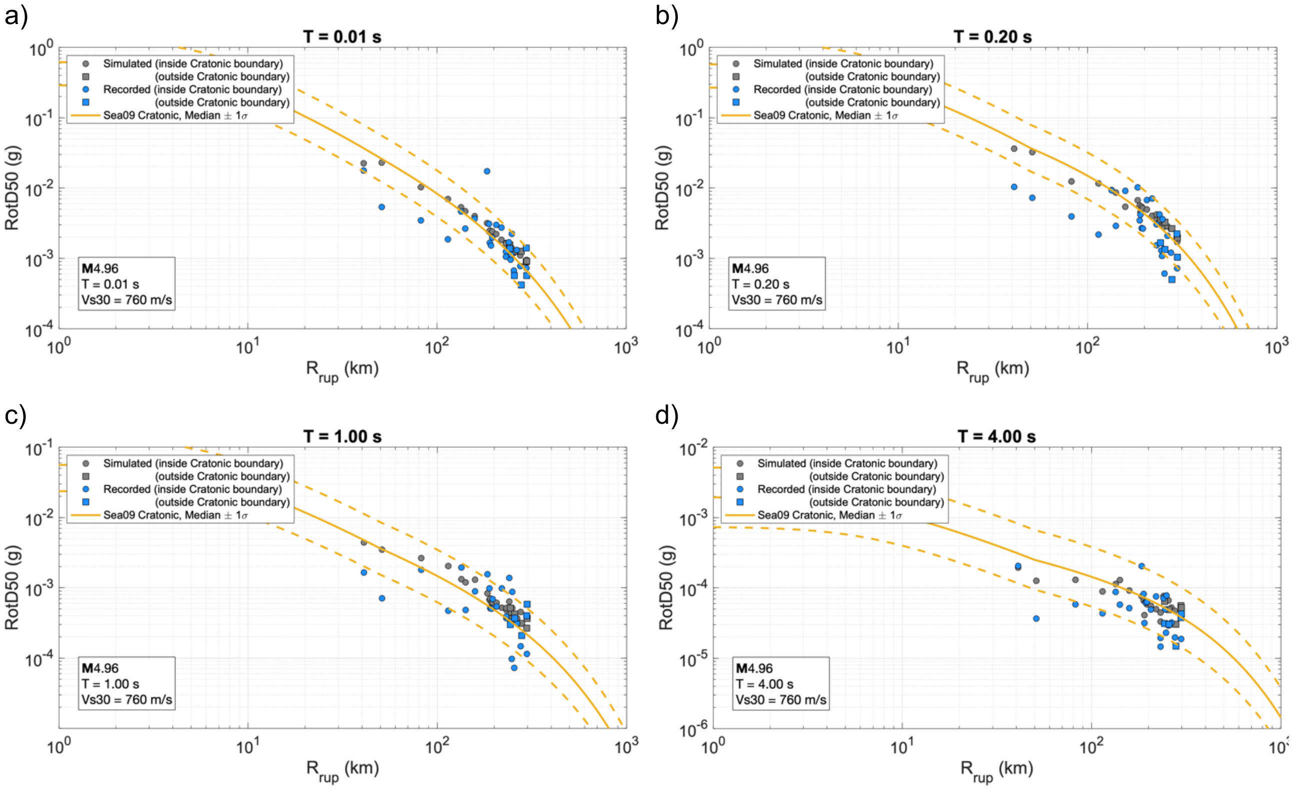

Figure 5. Distance attenuation of recorded (blue) and simulated (grey) RotD50 spectral acceleration at all sites with less than 300 km rupture distance, for four periods: (a) 0.01 sec (PGA), (b) 0.2 sec, (c) 1 sec, and (d) 4 sec.

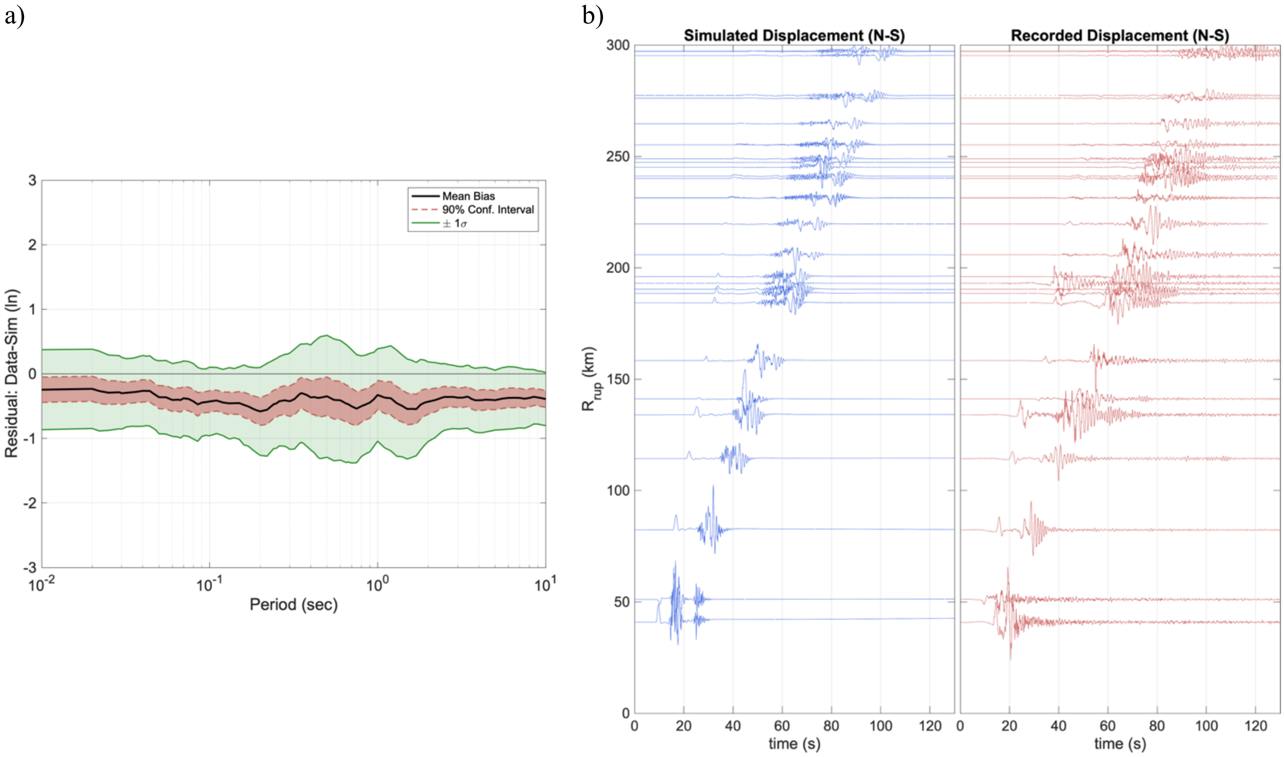

Figure 6. (a) The response spectral goodness-of-fit (GOF) summary for this earthquake simulation. (b) simulated and recorded displacement time series as a function of rupture distance.

Summary and Future Steps

This paper describes how the Sea09 ground motion model has changed, and as a result how SHA results for dam projects may be impacted. Comparisons with recently recorded ground motions in Australia have revealed that refinements to the distance and depth scaling components of the model provide a better fit to those data. The Sea09 models are distinct for Cratonic and non-Cratonic region earthquakes. Based on our ongoing evaluations of the newly acquired data, the path and site scaling components of the ground motions from both regions are similar, and most differences are related to source effects. As a result, we propose to update Sea09 with one model which incorporates the earthquake depth; accounting for the effects of R_g waves (from shallow events, impacting longer periods) and for energetic buried ruptures (impacting short periods).

This update involves broadband strong motion simulations to account for the effects of earthquake source and crustal structure properties of Australia; these are validated using the recorded ground motion data and are used to extrapolate the model to larger earthquake magnitudes that typically control design ground motions but for which no Australian data are available. These ongoing simulation validations use new data recorded in Cratonic Australia (Allen and Ghasemi, 2020).

The remaining Sea09 updates will be finalized once the validation phase is complete. We will run simulations for suites of scenarios events with a range of source depths and kinematic source realizations to develop a simulated ground motion database. Finally, the regression for ground motion model coefficients will be based on the combination of the scenario simulations and the recorded data. At this stage we will also evaluate and potentially adopt models for hanging wall effects and Vs30 scaling from others (e.g., Abrahamson et al., 2014; Stewart et al., 2021). Finally, we will update the Sea09 model for the aleatory variability based on the available data and on a review of global models (e.g., Goulet et al., 2014).

Acknowledgements

Thanks to Geoscience Australia (in particular, Trevor Allen and Hadi Ghasemi) for making the Cratonic region ground motion and source data publicly available, to David Love for sharing waveform data, first motion data, and magnitudes, focal depths and focal mechanisms of Cleve earthquakes, to Rob Graves and Arben Pitarka for providing input on the simulations, and to Sidao Ni for sharing the CAP code.

References

Abrahamson, N.A. and W.J. Silva (1997). Empirical response spectral attenuation relations for shallow crustal earthquakes. Seismological Research Letters 68, 94-127.

Abrahamson, N.A. and R.R. Youngs (1992). A stable algorithm for regression analysis using the random effects model. Bull. Seism. Soc. Am. 82, 505-510.

Abrahamson, N., W. Silva and R. Kamai (2014). Update of the AS08 Ground-Motion Prediction Equations Based on the NGA-West2 Data Set. Earthquake Spectra: August 2014, Vol. 30, No. 3, pp. 1025-1055.

Allen, T.I. (2012). Stochastic ground-motion prediction equations for southeastern Australian earthquakes using updated source and attenuation parameters. Geoscience Australia Record 2012/069.

Allen, T.I. (2018). The 2018 National Seismic Hazard Assessment for Australia: Data package: Maps and grid values. Geoscience Australia record 2018/33. Canberra, ACT, Australia

Allen, T., J. Griffin, M. Leonard, D. Clark and H. Ghasemi (2018). The 2018 National Seismic Hazard Assessment: Model overview. Record 2018/27. Geoscience Australia, Canberra. http://dx.doi.org/10.11636/Record.2018.027

Allen, T. I., Ghasemi, H. (2020). A Ground-Motion Database for Western and Central Australian Earthquakes: Provisional Dataset Prepared for the Seismic Hazard Assessment of the National Radioactive Waste Management Facility. Professional Opinion 2020/xx. Geoscience Australia, Canberra.

Atkinson, G.M. and Boore, D.M. (2006). Earthquake ground-motion prediction equations for eastern North America. Bull. Seism. Soc. Am., 96, 2181-2205.

Bayless J., P. Somerville, S. Condon, H.K. Thio, H. Ghasemi, T. Allen (2022). Updating the Somerville et al. (2009) Ground Motion Model for Cratonic Australia Using Broadband Ground Motion Simulations of Recently Recorded Cratonic Region Earthquakes. Proc. of the 2022 Australian Earthquake Engineering Society National Conference. 24-25 November 2022, Mount Macedon, Victoria, Australia.

Beresnev, I. A., and G. M. Atkinson (2002). Source parameters of earthquakes in eastern and western North America based on finite-fault modeling, Bull. Seis. Soc. Am. 92, 695–710.

Boore, D.M., J. P. Stewart, E. Seyhan, and G, M. Atkinson (2014). NGA-West2 Equations for Predicting Response Spectral Accelerations for Shallow Crustal Earthquakes, Earthquake Spectra 30, 1057-1085.

Boore, D.M. and K.W. Campbell (2017). Adjusting Central and Eastern North America Ground-Motion Intensity Measures between Sites with Different Reference-Rock Site Conditions. Bulletin of the Seismological Society of America; 107 (1): 132–148. doi: https://doi.org/10.1785/0120160208

Boore, D. M. (2015). Adjusting ground-motion intensity measures to a reference site for which Vs30 = 3000 m/s, PEER Report 2015/06, Pacific Earthquake Engineering Research Center, University of California, Berkeley, California, 85 pp.

Chiou, B.S.-J. and R.R. Youngs (2014). Update of the Chiou and Youngs NGA Ground Motion Model for Average Horizontal Component of Peak Ground Motion and Response Spectra, Earthquake Spectra 30, 1117-1153.

Clark, D, McPherson, A, Van Dissen, R (2012). Long-term behaviour of Australian stable continental region (SCR) faults. Tectonophysics 566–567: 1–30.

Ghasemi, H. and Allen, T. (2018). Selection and ranking of ground-motion models for the 2018 National Seismic Hazard Assessment of Australia: summary of ground-motion data, methodology and outcomes. Record 2018/29. Geoscience Australia, Canberra.

Gorbatov, A., K. Czarnota, B. Hejrani, M. Haynes, R. Hassan, A. Medlin, J. Zhao, F. Zhang, M. Salmon, H. Tkalcic, H. Yuan, M. Dentith, N. Rawlinson, A. Reading, B. Kennett, C. Bugden, and M. Costelloe (2020). AusArray: quality passive seismic data to underpin updatable national velocity models of the lithosphere; In, doi: 10.11636/135284.

Goulet, C.A, Bozorgnia, Y., Kuehn, N., Al Atik, L., Youngs, R.R., Graves, R.W. and Atkinson G.M. (2021). NGA-East Ground-Motion Characterization Model Part I: Summary of Products and Model Development. Earthquake Spectra, 37(S1): 1231–1282. https://doi.org/10.1177/87552930211018723

Graves R. W., Pitarka A. (2004). Broadband time history simulation using a hybrid approach, Proc. 13th World Conf. Earthq. Eng., Vancouver, Canada, paper no. 1098

Graves, R. W., Pitarka, A. (2010). Broadband ground-motion simulation using a hybrid approach, Bull. Seismol. Soc. Am. 100, 2095–2123, doi: 10.1785/0120100057.

Graves R. W., Pitarka A (2015). Refinements to the Graves and Pitarka (2010) Broadband Ground-Motion Simulation Method. Seismological Research Letters; 86 (1): 75–80. doi: https://doi.org/10.1785/0220140101

Hillis, R.R. & Reynolds, S.D.. (2000). The Australian Stress Map. Journal of the Geological Society. 157. 915-921. 10.1144/jgs.157.5.915.

Hoult, Ryan & Pascale, Adam & Jones, Abraham & Allen, Trevor. (2021). The MW 5.9 Woods Point Earthquake: A Preliminary Investigation of the Ground Motion Observations.

Kottke, A. (2018, July 27). arkottke/pyrotd v0.5.4 (Version v0.5.4). Zenodo. http://doi.org/10.5281/zenodo.1322849

Leonard, M. (2010). Earthquake Fault Scaling: Self-Consistent Relating of Rupture Length, Width, Average Displacement, and Moment Release. Bull. Seis. Soc. Am, 100, 1971-88.

Liang, J. Z., Hao, H., Gaull, B. A. and Sinadinovski, C. (2008). Estimation of Strong Ground Motions in Southwest Western Australia with a Combined Green's Function and Stochastic Approach, Journal of Earthquake Engineering, 12:3,382 – 405.

Maechling, P. J., F. Silva, S. Callaghan, and T. H. Jordan (2015). SCEC Broadband Platform: System Architecture and Software Implementation, Seismol. Res. Lett., 86, no. 1

Petersen, M. D., Shumway, A. M., Powers, P. M., Mueller, C. S., Moschetti, M. P., Frankel, A. D., et al. (2020). The 2018 update of the US national seismic hazard model: Overview of model and implications. Earthq. Spectra 36, 5–41. doi:10.1177/8755293019878199

Salmon, M, B. L. N. Kennett, E. Saygin (2013). Australian Seismological Reference Model (AuSREM): crustal component, Geophysical Journal International, Volume 192, Issue 1, January, 2013, Pages 190–206, https://doi.org/10.1093/gji/ggs004

Shea, H. N., and W. D. Barnhart (2022). The Geodetic Centroid (gCent) Catalog: global earthquake monitoring with satellite imaging geodesy, Bull. Seismol. Soc. Am., doi: 10.1785/0120220072.

Somerville, P.G., R.W. Graves, N.F. Collins, S.G. Song, S. Ni and P. Cummins (2009). Source and ground motion models of Australian earthquakes. Proceedings of the 2009 Annual Conference of the Australian Earthquake Engineering Society, Newcastle, Dec 11-13.

Somerville, P. and S. Ni (2010). Contrast in Seismic Wave Propagation and Ground Motion Models between Cratonic and Other Regions of Australia. In Proceedings of the Australian Earthquake Engineering Society, 2010 Conference.

Stewart, J. P., G.A. Parker, G.M. Atkinson, D.M. Boore, Y.M.A. Hashash, and W.J. Silva (2020). Ergodic site amplification model for central and eastern North America. Earthquake Spectra 36 (1), 42-68.

Thompson, E. M., and C. B. Worden (2017). Estimating rupture distances without a rupture, Bulletin of the Seismological Society of America. https://doi.org/10.1785/0120170174.

Tan, Y., A Song, S Wei, D Helmberger (2010) Surface Wave Path Corrections and Source Inversions in Southern California. Bulletin of the Seismological Society of America; 100 (6): 2891–2904. doi: https://doi.org/10.1785/0120090063

Toro, G.R., N.A. Abrahamson, and J.F. Schneider (1997). Model of strong ground motions from earthquakes in central and eastern North America: best estimates and uncertainties. Seismological Research Letters, 68(1), 41-57.

Zhao, L. S., and D. V. Helmberger (1994). Source estimation from broadband regional seismograms, Bull. Seismol. Soc. Am., 84, 91–104.

Zhu, L. and L.A. Rivera (2002). A note on the dynamic and static displacements from a point source in multilayered media, GJI, 148:3, 619–627.